

Analysis of thermo-elastic problems using the improved element-free Galerkin method

Imen Debbabi¹ · Hédi BelhadjSalah¹

Received: 17 May 2016 / Revised: 7 October 2016 / Accepted: 12 November 2016 /
Published online: 30 November 2016
© SBMAC - Sociedade Brasileira de Matemática Aplicada e Computacional 2016

Abstract The improved element-free Galerkin method (IEFG) is presented to deal with thermo-elastic problems. This mesh-free method is a combination between the element-free Galerkin method and the improved moving least-square approximation. It has not the Kronecker delta property, and the penalty method is used to impose the essential boundary conditions. In this paper, linear and stationary thermo-elasticity is treated. To solve the thermo-elastic problem, this latter is decoupled into two separate parts: first, the heat transfer problem is analyzed to reach the temperature field, which is used as input in the mechanical problem to calculate the displacement field and then the stress fields. Numerical examples with different boundary conditions are illustrated. The performance and the accuracy of the IEFG method are approved when obtained results are compared to finite-element results and analytical solution.

Keywords Mesh free methods · Element free Galerkin method (EFG) · Improved element free Galerkin method (IEFG) · Moving least square approximation (MLS) · Improved moving least square approximation (IMLS) · Linear thermo-elasticity

Mathematics Subject Classification 74F05 · 35Q79 · 65N35 · 65Z05

1 Introduction

Thermo-elasticity and especially structure's failure due to thermal stresses is related to many engineering problems (Takeuti and Furukawa 1981; Hibbitt and Marcal 1973). Thermo-

Communicated by Jorge X. Velasco.

✉ Imen Debbabi
imen.debbabi86@gmail.com

Hédi BelhadjSalah
hedi.belhadjsalah1@gmail.com

¹ Laboratory of Mechanical Engineering, National School of Engineering, University of Monastir, Monastir, Tunisia

elasticity has for purpose to compute the behavior of an elastic body under thermal and mechanical loads. The linear or weakly coupled thermo-elasticity is solved in two steps: first, the temperature field is computed when solving the heat transfer problem, and then, it is introduced in the mechanical equation to calculate the displacement and stress fields (Parkus 1968).

The lack of analytic solution for thermo-elastic problems, justify the fact that most of thermo-elastic problems are treated using numerical methods. In this way, several numerical methods have been used and developed. Beginning with finite-element method (FEM) which has been the most widely and successfully used for long time (Huebner and Dewhirst 2008; Zenkour and Abbas 2014; Reza Eslami 2014), coming to mesh-free methods which has, recently, attracted much attention thanks to their ability to deal with conventional method's limitations. These latter are in fact always related to remeshing and adaptive analysis. Hence, varieties of mesh-free methods have been presented, and have shown their ability to solve thermo-elastic problems. For instance, Local Boundary Integral Equation (LBIE) method has been used by Sladek to solve 2D stationary thermo-elasticity (Sladek et al. 2001). Functionally Graded materials under thermal and mechanical stresses have been studied with different mesh-free methods (Ching and Yen 2005; Feng and Cui 2013). In this way also, to study 2D solid under thermo-mechanical loads, Ching developed the Meshless Local Petrov-Galerkin method (MLPG) (Ching and Chen 2007). Zheng and Gao used the MLPG method too to treat the thermo-elastic shock modeling (Zheng and Gao 2015). The EFG method, one of the famous and widely used mesh-free methods, has shown its ability to solve thermo-mechanical problems: the shape sensitivity of thermo-elastic solid has been treated by Bubaruu and Mukherjee (Bobaruu and Mukherjee 2002). Likewise, this method had been successfully utilized by Singh to treat first, crack problems under thermo-mechanical load (Pant and Singh 2010, 2011) then, after studying the Fatigue crack growth under thermo-elastic loading with an extended finite-element method, he developed the EFG method to investigate the fatigue crack growth (Pathak and Singh 2013, 2014). In this context, Bouhala used an extended EFG method to study the thermal and thermo-mechanical influence on the crack propagation (Bouhala and Makradiand 2012).

Close to the EFG, The Improved Element-Free Galerkin (IEFG) method is a combination of the EFG method with the Improved Moving Least-Square (IMLS) approximation. This meshless method has improved its efficiency and computational speed in many works (Zhang and Zhao 2009; Zhang and Wang 2013; Cheng and Liew 2012). Indeed, in the IMLS approximation, weighted orthogonal basis functions are used to construct the shape functions; for this reason, the problem's solution is obtained without matrix inversion in the system's equations, and hence, the computational speed of the method is justified (Liew and Cheng 2005; Zhang and Liew 2014; Zeng and Peng 2011; Debbabi and Sendi 2015). Despite its efficiency and computational speed, the IEFG method has not been applied to treat thermo-elasticity; for this reason, the IEFG method is presented to study linear thermo-elasticity in this work.

In this paper, the IMLS approximation is first introduced, and then, the IEFG method is discussed for linear thermo-elasticity and governing equations are presented. Finally, the accuracy and the efficiency of the method are illustrated using 2D numerical examples. To validate the capacity of the IEFG method, results are compared to analytic solution when it is available. In the case of the lack of the analytical solution, results are compared to a reference solution obtained using the FEM commercial software "ABAQUS" in which a large number of fine meshes is adopted.

2 The IMLS approximation

In the IMLS approximation for a field variable $u(x)$ defined in the domain Ω , the approximation of $u(x)$ denoted $u^h(x)$ is

$$u^h(x) = \sum_{i=1}^m p_i(x)a_i(x) = p^T(x)a(x) \tag{1}$$

where m is the number of terms in the basis weighted orthogonal vector $p(x)$ and $a(x)$ is a vector of coefficients of the basis functions.

In the IMLS, the basis function sets $p_1(x), p_2(x), \dots, p_m(x)$ are considered to be weighted orthogonal polynomials set with the weight function $\{w_i\}$ about point $\{x_i\}$ if the condition (2), given in the following, is satisfied:

$$(p_k, p_j) = \sum_{i=1}^n w_i p_k(x_i)p_j(x_i) = \begin{cases} 0, & k \neq j \\ a_k, & k = j \end{cases} (k, j = 1, 2 \dots m) \tag{2}$$

To reach the vector of coefficients $a^T(x) = (a_1(x), a_2(x), \dots, a_m(x))$ and obtain the approximation of $u(x)$, the difference between $u^h(x)$ and $u(x)$ is minimized using a weighted least-square method.

J is a function defined as follows:

$$\begin{aligned} J(a, x) &= \sum_I^n w(x - x_I) [u^h(x, x_I) - u(x_I)]^2 \\ &= \sum_I^n w(x - x_I) \left[\sum_{i=1}^m p_i(x_I) a_i(x) - u(x_I) \right]^2 \end{aligned} \tag{3}$$

where $W(x - x_I)$ is the weight function associated with the node I , this weight function is nonzero only over a small neighborhood of a node x_I called the domain of influence and $x_I, I = 1, 2, \dots, n$ are nodes in this domain of influence that cover x . In the present work, the fourth-order spline weight function is chosen (Li et al. 2013):

$$w(s) = \begin{cases} 1 - 6s^2 + 8s^3 - 3s^4, & |s| \leq 1 \\ 0 & |s| \geq 1 \end{cases} \tag{4}$$

where $s = \frac{\|x - x_I\|}{d}$ in which $\|x - x_I\|$ is the distance from a sampling point x to a node x_I , and d is the size of the domain of influence of the I th node.

In the case of a circular domain, $d = a_c d_i$, where a_c is a scaling parameter, and d_i is the average distance between nodes.

A matrix formulation of Eq. (3) is given by

$$J(a, x) = (pa(x) - u)^T W(x) (pa(x) - u). \tag{5}$$

Knowing that

$$u^T = (u_1, u_2, \dots, u_n) \quad \text{and} \quad u_i = u(x_i) \tag{6}$$

$$p = \begin{bmatrix} p_1(x_1) & p_2(x_1) & \dots & p_m(x_1) \\ p_1(x_2) & p_2(x_2) & \dots & p_m(x_2) \\ \vdots & \vdots & \ddots & \vdots \\ p_1(x_n) & p_2(x_n) & \dots & p_m(x_n) \end{bmatrix} \tag{7}$$

$$W(x) = \begin{bmatrix} w(x - x_1) & 0 & \dots & 0 \\ 0 & w(x - x_2) & \dots & 0 \\ \vdots & \vdots & \ddots & \vdots \\ 0 & 0 & \dots & w(x - x_n) \end{bmatrix}. \tag{8}$$

By setting $\frac{\partial J(a,x)}{\partial a} = 0$, the following system equations are obtained:

$$A(x)a(x) = B(x)u \tag{9}$$

where $A(x)$ is called the moment matrix and $B(x)$ is a vector defined by

$$A(x) = p^T W(x)p \tag{10}$$

$$B(x) = p^T W(x). \tag{11}$$

When the condition (2) is considered, Eq. (9) can be written as follows:

$$\begin{bmatrix} (p_1, p_1) & 0 & \dots & 0 \\ 0 & (p_2, p_2) & & 0 \\ \vdots & \vdots & \ddots & \vdots \\ 0 & 0 & \dots & (p_m, p_m) \end{bmatrix} \begin{bmatrix} a_1(x) \\ a_2(x) \\ \vdots \\ a_m(x) \end{bmatrix} = \begin{bmatrix} (p_1, u_1) \\ (p_2, u_1) \\ \vdots \\ (p_m, u_1) \end{bmatrix}. \tag{12}$$

The moment matrix becomes diagonal and coefficients a_i are obtained directly using the following expression:

$$a_i(x) = \frac{(p_i, u_1)}{(p_i, p_i)} \quad (i = 1, 2, \dots, m). \tag{13}$$

Then

$$a(x) = \bar{A}(x)B(x)u \tag{14}$$

where

$$\bar{A}(x) = \begin{bmatrix} \frac{1}{(p_1, p_1)} & 0 & \dots & 0 \\ 0 & \frac{1}{(p_2, p_2)} & \dots & 0 \\ \vdots & \vdots & \ddots & \vdots \\ 0 & 0 & \dots & \frac{1}{(p_m, p_m)} \end{bmatrix}. \tag{15}$$

Going back to the u^h approximation, this latter can be given as follows:

$$u^h(x) = \bar{\Phi}(x)u = \sum_I^n \bar{\Phi}_I(x)u_I \tag{16}$$

where $\bar{\Phi}(x)$ is the vector of IMLS shape functions defined by

$$\bar{\Phi}(x) = p^T(x)\bar{A}(x)B(x). \tag{17}$$

When compared to the presented IMLS approximation, the main difference between the traditional MLS approximation, where the same approach is used to get shape functions, is that basis functions in the MLS approximation are not weighted orthogonal, so that the condition (2) is not satisfied. This difference leads to a non-diagonal moment matrix in Eq.

(9) when traditional approximation is adopted. When the moment matrix is not diagonal, its inversion is not simple and it is a time-consuming operation (Zhang and Zhao 2009).

3 Governing equations of linear thermo-elasticity

The IIEFG method is a Galerkin scheme using the IMLS shape functions, and the numerical integration is evaluated on background cells (Belytschko and Lu 1994). This method is applied to the above 2D thermo-elastic problem, which will be solved in two separates parts, the heat transfer problem followed by the mechanical one.

3.1 Formulation of the heat transfer problem

Governing equations of the stationary heat transfer problem for an isotropic domain Ω bounded by $\Gamma = \Gamma_1 \cup \Gamma_2 \cup \Gamma_3$ are given as follows:

$$k\nabla^2 T + Q = 0 \tag{18}$$

where T define the temperature field, k is the thermal conductivity, and Q is the heat source. The boundary conditions associated with this problem are

Dirichlet boundary conditions:

$$T = \bar{T}, \quad \text{on } \Gamma_1. \tag{19}$$

Neumann boundary

$$n\nabla T = \bar{q}, \quad \text{on } \Gamma_2. \tag{20}$$

Robin boundary

$$n\nabla T = h(T - T_\infty), \quad \text{on } \Gamma_3 \tag{21}$$

where n is the outward normal to the boundary Γ . h is the convective heat transfer coefficient, \bar{q} is the prescribed heat flux, and T_∞ represents the surrounding fluid's temperature.

After multiplication of Eq. (18) by the test function T^* and using the flux- divergence theorem in addition to the integration by parts, the variational formulation based on the IIEFG discretization is given as follows:

$$\int_{\Omega} \nabla T^* k \nabla T d\Omega = \int_{\Omega} T^* Q d\Omega + \int_{\Gamma_2} T^* \bar{q} d\Gamma + \int_{\Gamma_3} T^* h (T - T_\infty) d\Gamma. \tag{22}$$

The shape functions of the IMLS approximation do not have the Delta Kronecker property, so to impose the boundary conditions, penalty technique is used (Zhu and Atluri 1998) and Eq. (22) becomes

$$\int_{\Omega} \nabla T^* k \nabla T d\Omega + \gamma \int_{\Gamma_1} T^* (T - \bar{T}) d\Gamma = \int_{\Gamma_2} T^* \bar{q} d\Gamma + \int_{\Gamma_3} T^* h (T - T_\infty) d\Gamma \tag{23}$$

where γ used in the latter equation is the penalty coefficient, which can be considered as $10^{4-13} \times \max(\text{diagonal elements in the stiffness matrix})$ (Liu 2003).

The use of the discretization (16), the system equation of the heat transfer problem, is obtained as

$$[\bar{K}]\{T\} = \{\bar{F}\} \tag{24}$$

$$[\bar{K}] = [K] + [H] + [K^\gamma] \tag{25}$$

$$\{\bar{F}\} = \{F\} + \{F^\gamma\} \tag{26}$$

where

$$K_{IJ} = \int_{\Omega} \bar{\Phi}_{I,x_1} k \bar{\Phi}_{J,x_1} + \bar{\Phi}_{I,x_2} k \bar{\Phi}_{J,x_2} d\Omega \tag{27}$$

$$H_{IJ} = \int_{\Gamma_3} \bar{\Phi}_I h \bar{\Phi}_J d\Gamma \tag{28}$$

$$K_{IJ}^\gamma = \int_{\Gamma_1} \bar{\Phi}_I \gamma \bar{\Phi}_J d\Gamma \tag{29}$$

$$F_I = \int_{\Omega} \bar{\Phi}_I Q d\Omega + \int_{\Gamma_2} \bar{\Phi}_I \bar{q} d\Gamma + \int_{\Gamma_3} \bar{\Phi}_I h T_\infty d\Gamma \tag{30}$$

$$F_I^\gamma = \int_{\Gamma_1} \bar{\Phi}_I \gamma \bar{T} d\Gamma. \tag{31}$$

3.2 Formulation of the thermo-elastic problem

The temperature field is obtained using Eq. (24) and it can be used in the following linear thermo-elastic problem:

$$\nabla \sigma + f - \alpha \nabla \theta = 0, \quad \text{in } \Omega \tag{32}$$

$$u = \bar{u}, \quad \text{in } \Gamma_u \tag{33}$$

$$\sigma \cdot n = \bar{t} + \alpha \theta n, \quad \text{in } \Gamma_t \tag{34}$$

in which σ , f , θ , α , u , \bar{u} , n and \bar{t} are, respectively, the stress tensor, the body force, the change in temperature, the coefficient of linear thermal expansion, displacement field, the imposed displacement, the outward normal vector, and the stress boundary.

Proceeding in the same way as in the heat transfer problem, using the test function v^* and imposing the boundary conditions (33) and (34), the variational formulation of the thermo-elastic problem is obtained as

$$\begin{aligned} \int_{\Omega} \sigma \varepsilon^* d\Omega + \gamma \int_{\Gamma_u} uv^* d\Gamma &= \int_{\Omega} f v^* d\Omega + \int_{\Gamma_t} \bar{t} v^* d\Gamma - \gamma \int_{\Gamma_u} \bar{u} * v^* d\Gamma \\ &+ \int_{\Omega} \beta \theta \text{div}(v^*) d\Omega - \int_{\Gamma_u} \beta \theta n v^* d\Gamma \end{aligned} \tag{35}$$

where

$$\{\sigma\} = [H^e] \{\varepsilon\}. \tag{36}$$

Introducing

$$u = \{U\} = [\bar{\phi}] \{U_n\} \quad \text{and} \quad v^* = \{V^*\} = [\bar{\phi}] \{V_n^*\}. \tag{37}$$

The strain-displacement relation is

$$\{\varepsilon\} = [B^e] \{U_n\} \quad \text{and} \quad \{\varepsilon^*\} = [B^e] \{V_n^*\} \tag{38}$$

where

$$[B^e] = [D^e] [\bar{\phi}] = \begin{bmatrix} \frac{\partial}{\partial x} & 0 \\ 0 & \frac{\partial}{\partial y} \\ \frac{\partial}{\partial y} & \frac{\partial}{\partial x} \end{bmatrix} \begin{bmatrix} \bar{\phi}_1 & 0 & \bar{\phi}_2 & 0 & \dots & \bar{\phi}_n & 0 \\ 0 & \bar{\phi}_1 & 0 & \bar{\phi}_2 & \dots & 0 & \bar{\phi}_n \end{bmatrix} \tag{39}$$

In plane stress:

$$[H^e] = \frac{E}{(1 - \nu^2)} \begin{bmatrix} 1 & \nu & 0 \\ \nu & 1 & 0 \\ 0 & 0 & \frac{1-\nu}{2} \end{bmatrix} \quad \text{and} \quad \beta = \frac{\alpha^* E}{1-\nu}. \tag{40}$$

In plane strain

$$[H^e] = \frac{E}{(1 - 2\nu)(1 + \nu)} \begin{bmatrix} 1 - \nu & \nu & 0 \\ \nu & 1 - \nu & 0 \\ 0 & 0 & \frac{1-2\nu}{2} \end{bmatrix} \quad \text{and} \quad \beta = \frac{\alpha^* E}{1-2\nu} \tag{41}$$

where E is the Young's modulus and ν is the Poisson's ratio.

The discretization (16) allows us to have the above system matrix:

$$\begin{aligned} & \int_{\Omega} [B^e]^T [H^e] [B^e] \{U_n\} d\Omega + \gamma \int_{\Gamma_u} [\bar{\phi}]^T [\bar{\phi}] \{U_n\} d\Gamma \\ & = \int_{\Omega} [\bar{\phi}]^T f d\Omega + \int_{\Omega} \beta \theta [\check{D}] d\Omega + \int_{\Gamma_t} [\bar{\phi}]^T \bar{t} d\Gamma \\ & + \gamma \int_{\Gamma_u} [\bar{\phi}]^T \bar{u} d\Gamma - \int_{\Gamma_u} \beta \theta [\bar{\phi}]^T n d\Gamma \end{aligned} \tag{42}$$

in which

$$[\check{D}] = \left[\frac{\partial \bar{\phi}_1}{\partial x_1}, \frac{\partial \bar{\phi}_1}{\partial x_2}, \dots, \frac{\partial \bar{\phi}_n}{\partial x_1}, \frac{\partial \bar{\phi}_n}{\partial x_2} \right]. \tag{43}$$

The matrix equation system resulting from Eq. (42) is

$$[\bar{K}] \{U_n\} = \{\bar{F}\} \tag{44}$$

where

$$[\bar{K}] = [K] + [K^\gamma] \tag{45}$$

$$\{\bar{F}\} = \{F\} + \{F^\gamma\} \tag{46}$$

$$[K] = \int_{\Omega} [B^e]^T [H^e] [B^e] d\Omega \tag{47}$$

$$[K^\gamma] = \int_{\Gamma_u} [\bar{\phi}]^T \gamma [\bar{\phi}] d\Gamma \tag{48}$$

$$\{F\} = \int_{\Omega} [\bar{\phi}]^T f \, d\Omega + \int_{\Omega} \beta\theta [\check{D}] \, d\Omega + \int_{\Gamma_i} [\bar{\phi}]^T \bar{t} \, d\Gamma - \int_{\Gamma_u} \beta\theta [\bar{\phi}]^T n \, d\Gamma \quad (49)$$

$$\{F^\gamma\} = \int_{\Gamma_u} \gamma [\bar{\phi}]^T \bar{u} \, d\Gamma. \quad (50)$$

To evaluate the integrals, the studied domain Ω is discretized into background cells: quadrangles cells used only for integration. Using the Gauss quadrature rule, the global integration can be written as

$$\int_{\Omega} G \, d\Omega = \sum_{k=1}^{n_c} \int_{\Omega_k} G \, d\Omega = \sum_{k=1}^{n_c} \sum_{i=1}^{n_g} w_i G(x_{Qi}) \left| J_{ik}^D \right| \quad (51)$$

where n_c is the number of quadrangles cells and Ω_k represents the domain of the k^{th} quadrangle cell in which n_g is the number of Gauss points used. G is the integrand and the Gauss weighting factor, associated with the i^{th} Gauss point at x_{Qi} , is w_i and $|J_{ik}^D|$ represents the Jacobian matrix for the integration area of the quadrangle cell k . Similarly, the Gauss quadrature rule is used on the boundary Γ .

4 Numerical examples

To improve the performance and the accuracy of the present mesh-free method for linear thermo-elasticity, some numerical examples are investigated. In the first one, the problem is chosen with analytical solution, and then, the treated thermo-elastic problem do not have analytical solution and results are compared to a reference FEM ones, obtained with a large number of fine meshes. The efficiency of the IIEFG is validated for both regular and irregular node distributions.

4.1 A hollow cylinder

As a first example, we consider a hollow cylinder under thermal gradient discussed by Sladek using LBIE on 2001. The temperatures imposed on the internal and external surfaces of the hollow cylinder are constant but different. This cylinder can be treated as a thermo-elastic problem with plane strain condition. Thanks to the symmetry of the proposed problem, we compute only a quarter of the cylinder, as shown in Fig. 1.

Analytical solution of this problem is given for temperature and hoop stresses as follows (Sladek et al. 2001):

$$T(r) = T_1 + \frac{\Delta T}{Ln(\frac{R_2}{R_1})} Ln\left(\frac{r}{R_1}\right) \quad (52)$$

$$\sigma_{\varphi\varphi}(r) = \Delta T \frac{E\alpha}{2(1-\nu)} \left[\frac{1 + \frac{1}{\left(\frac{r}{R_1}\right)^2}}{1 - \left(\frac{R_1}{R_2}\right)^2} + \frac{1 + Ln\left(\frac{r}{R_1}\right)}{Ln\left(\frac{R_1}{R_2}\right)} \right]. \quad (53)$$

In computation, cylinder radii are $R_1 = 1$ mm and $R_2 = 3$ mm. Material's characteristics are elasticity modulus $E = 2E5$ MPa, poisson ratio $\nu = 0.25$, and coefficient of thermal expansion $\alpha = 1.67E - 5^\circ K^{-1}$. For the numerical analysis, we used a regular repartition of 41×41 nodes, as presented in Fig. 2.

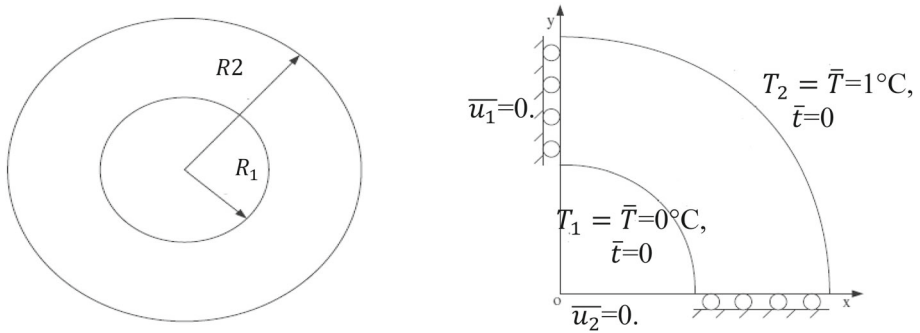


Fig. 1 Geometry and boundary conditions of the cylinder

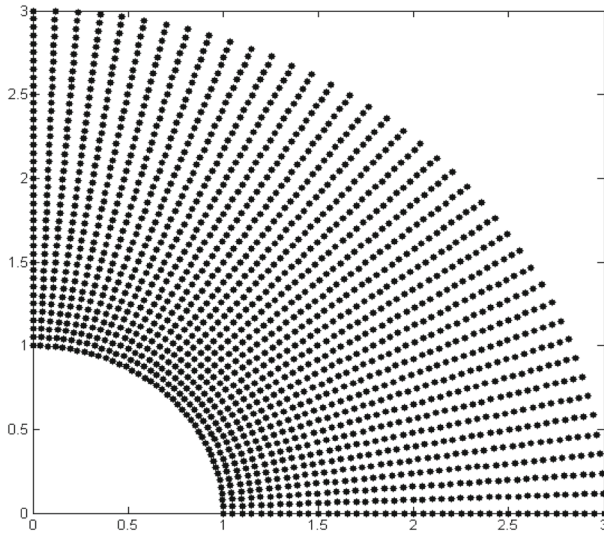


Fig. 2 Regular nodes repartition

The size of the domain of influence used in computation is $d = 0.06$ mm using a scaling parameter $a_c = 1.2$ for thermal analysis and $d = 0.095$ mm with $a_c = 1.8$ for mechanical analysis. Next, we use polar coordinate system (r, φ) to present different results.

To validate the developed IIEFG program, L2 relative error norm is verified for temperature and hoop stress all over the studied domain: for temperature field, L2 relative error norm is equal to 5.26710^{-4} , and for hoop stress field, it is equal to 1.29210^{-2} .

From Fig. 3, the efficiency of the IIEFG method to treat the heat transfer problem and give a temperature evolution in good agreement with the analytical one is proved. Indeed, the relative error begins about 0.05% and it decreases to be under 0.01% for $\varphi = 0$. The expression of the relative error used in the following curves is given by

$$\text{Relative error} = \frac{|u^{IIEFG} - u^{anal}|}{\max(|u|^{anal})} \tag{54}$$

In case of the lack of analytical solution, we use a reference solution to calculate the relative error.

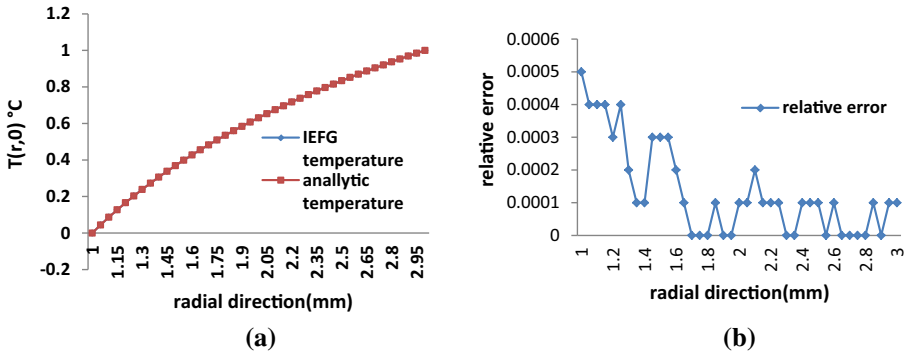


Fig. 3 a Temperature evolution for $\varphi = 0$, b Relative error for temperature distribution at $\varphi = 0$

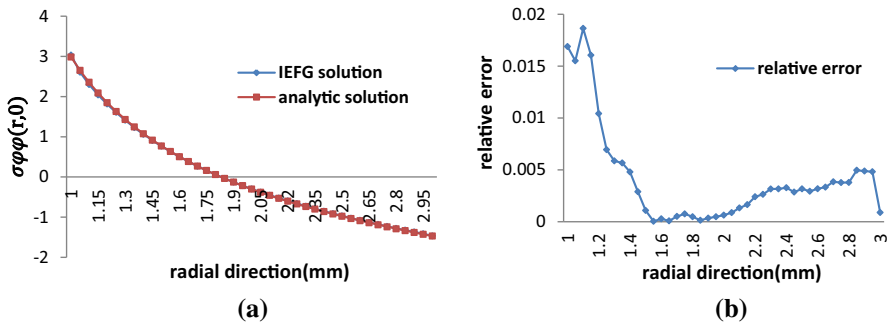


Fig. 4 a Hoop stresses evolution for $\varphi = 0$, b Relative error for hoop stress for $\varphi = 0$

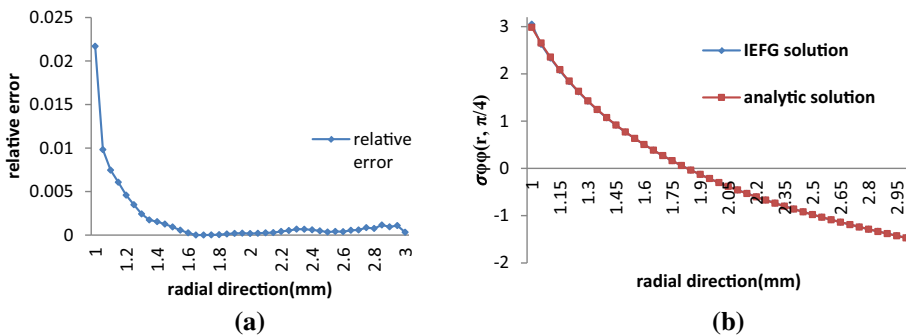


Fig. 5 a Hoop stresses evolution for $\varphi = \frac{\pi}{4}$, b Relative error for hoop stress for $\varphi = \frac{\pi}{4}$

To show the performance of the IIEFG method for thermo-elastic resolution, hoop stress evolution for $\varphi = 0$, $\varphi = \frac{\pi}{4}$, and $\varphi = \frac{\pi}{2}$ along radial direction are, respectively, as presented in Figs. 4, 5, and 6. The error begins relatively high near the internal radii, and it decreases to be less than 1% in the rest of the domain. Since the relative error has been under 4% for the three presented cases, we can conclude that the IIEFG method agree well again with analytic results.

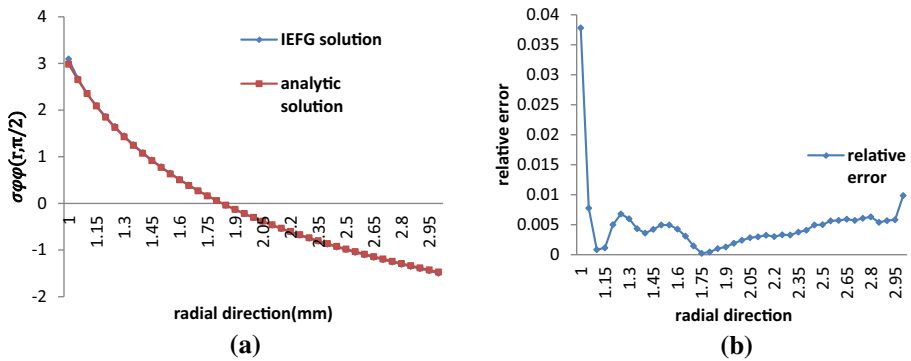


Fig. 6 a Hoop stresses evolution for y direction for $\varphi = \frac{\pi}{2}$. b Relative error for hoop stress for $\varphi = \frac{\pi}{2}$

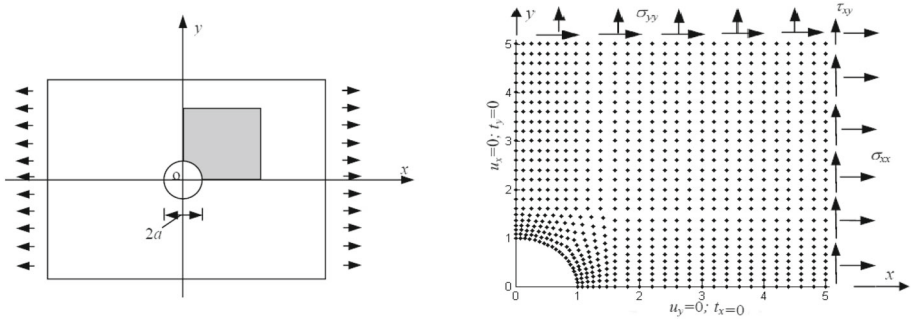


Fig. 7 Geometry, nodes distribution, and boundary conditions of the problem

4.2 An infinite plate with a circular hole under thermal and mechanical loads

In this section, an infinite plate subjected to a unidirectional traction load is discussed to validate the applicability of the IEFG method for 2D thermo-elasticity. The infinite plate is computed as a quarter finite one due to the symmetry of the problem. Both thermal and mechanical boundary conditions are imposed. All sides of the plate are subjected to a constant temperature of 600°K. On the left and bottom edges, symmetry conditions are assumed. The inner boundary is traction free, and Neumann mechanical boundary conditions assumed are shown in Fig. 7 and given as follows:

$$\sigma_{xx} = 1 - \frac{a^2}{r^2} \left(\frac{3}{2} \cos(\theta) + \cos(4\theta) \right) + \frac{3}{2} \frac{a^4}{r^4} \cos(4\theta) \tag{55}$$

$$\sigma_{yy} = -\frac{a^2}{r^2} \left(\frac{1}{2} \cos(2\theta) - \cos(4\theta) \right) - \frac{3}{2} \frac{a^4}{r^4} \cos(4\theta) \tag{56}$$

$$\sigma_{xy} = -\frac{a^2}{r^2} \left(\frac{1}{2} \sin(2\theta) + \sin(4\theta) \right) + \frac{3}{2} \frac{a^4}{r^4} \sin(4\theta). \tag{57}$$

Fig. 8 Temperature evolution for $\varphi = \frac{\pi}{2}$

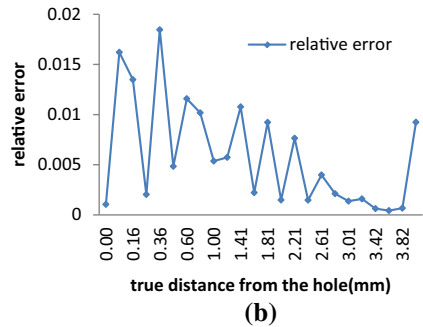
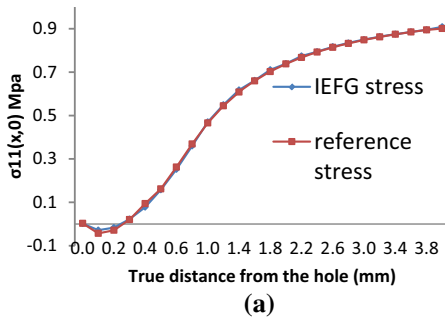
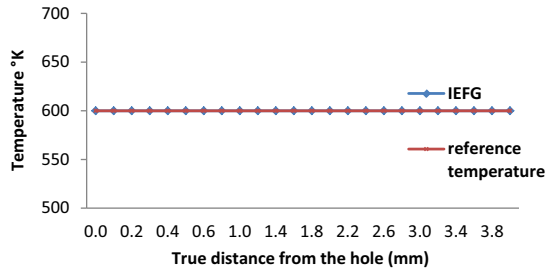


Fig. 9 a Stress σ_{11} for $y = 0$ mm b relative error for $y = 0$ mm

Material’s parameters used in the computation are Young modulus $E = 2E5\text{Mpa}$, Poisson ratio $\nu = 0.25$, and coefficient of thermal expansion $\alpha = 1.2E-5^\circ\text{K}^{-1}$. Plain strain condition is considered for this problem.

A number of 810 Irregular nodes distribution are presented: a large number of nodes are localized near to the hole and regular one in the rest of the domain, as presented in Fig. 7. The scaling parameter for thermal problem is equal to 1.2, and it is equal to 2.1 for thermo-mechanical analysis. To verify the efficiency of the IIEFG method, results are compared to a reference solution, obtained with ABAQUS using very dense mesh.

The accuracy of the developed IIEFG method is verified, first, by calculating the L2 relative error norm between reference solutions, FEM solution calculated with a very dense mesh, and the IIEFG ones, and then stress and displacement examined throughout several paths. Hence, the L2 relative error norm is equal to 6.24410^{-2} when stress is checked and it is equal to 2.71810^{-4} when displacement is studied. For the temperature, as shown in Fig. 8, curves are combined and the relative error is inconsiderable.

The stress σ_{11} obtained using the IIEFG method is compared to the reference one for several paths: Figs. 9 and 10 represent the evolution of σ_{11} , respectively, for $y = 0$ mm and $x = 0$ mm. For these two cases, the relative error between the IIEFG and the FEM methods is less than 2%. In addition, the evolution of σ_{11} on the hole’s boundary (inner boundary), plotted on Fig. 11, shows that the IIEFG method is able to reproduce good stress with a relative error under 3% all over the inner boundary.

The ability of the IIEFG to give accurate results for displacement is also discussed. This mesh-free method gives displacements with relative error under $2.1E-6$. Indeed, displacement u_x for $y = 0$ mm and displacement u_y for $x = 0$ mm are plotted with reference displacements, respectively, in Figs. 12a and 13a and it is clear that mesh-free results are in excellent agreement with reference ones.

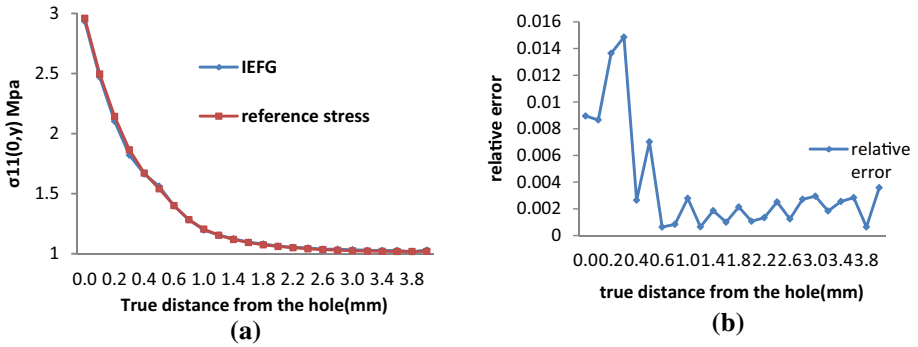


Fig. 10 a Stress σ_{11} for $x = 0$ mm. b Relative error for $x = 0$ mm

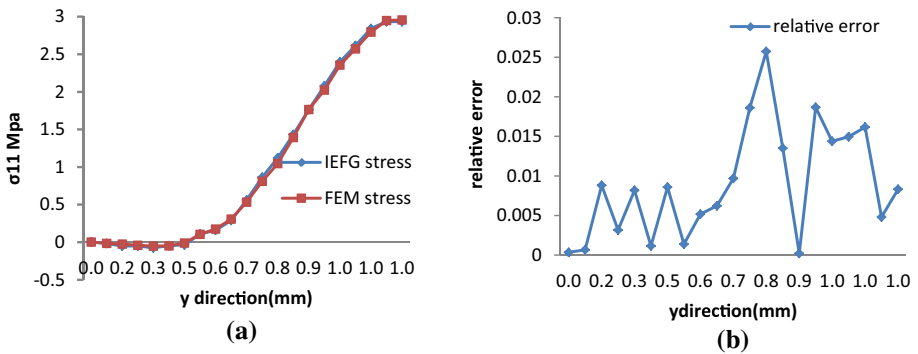


Fig. 11 a σ_{11} evolutions on the hole's boundary. b Relative error associated

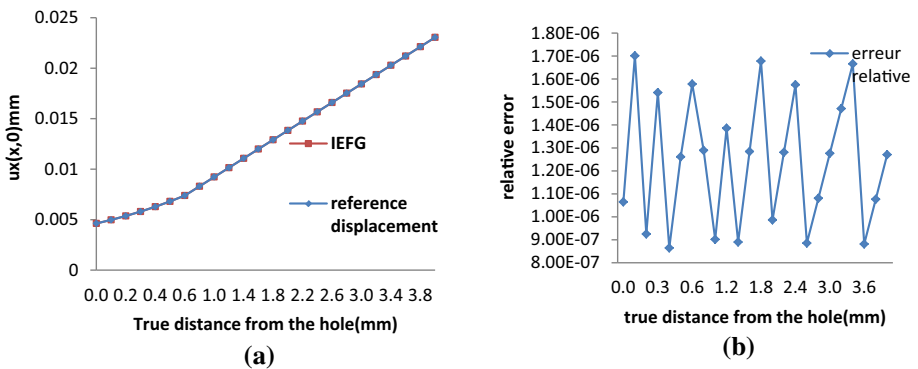


Fig. 12 a Displacement u_x for $y = 0$ mm, b Relative error for $y = 0$ mm

To demonstrate the numerical performance of the IEFG method, u_x evolution and σ_{22} evolution all over the plate are presented, respectively, in Figs. 14a and 15a, close agreement is detected when results are compared to the reference ones, and FEM solution obtained using a very dense mesh is presented, respectively, in Figs. 14b and 15b.

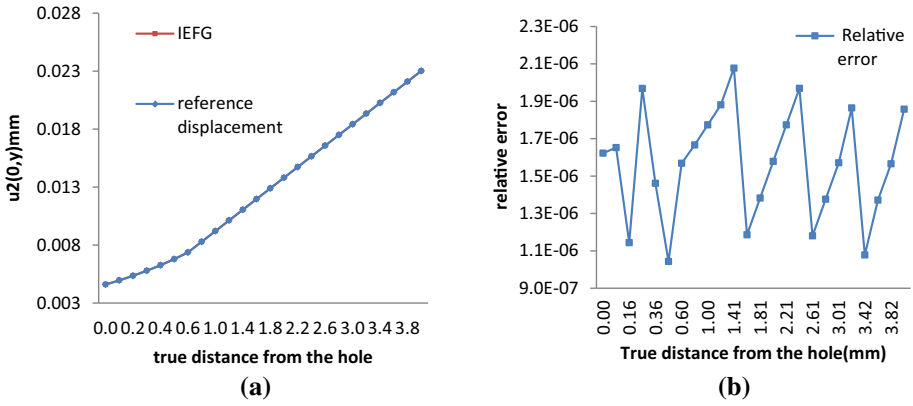


Fig. 13 **a** Displacement u_2 for $x = 0$ mm. **b** Relative error for $x = 0$ mm

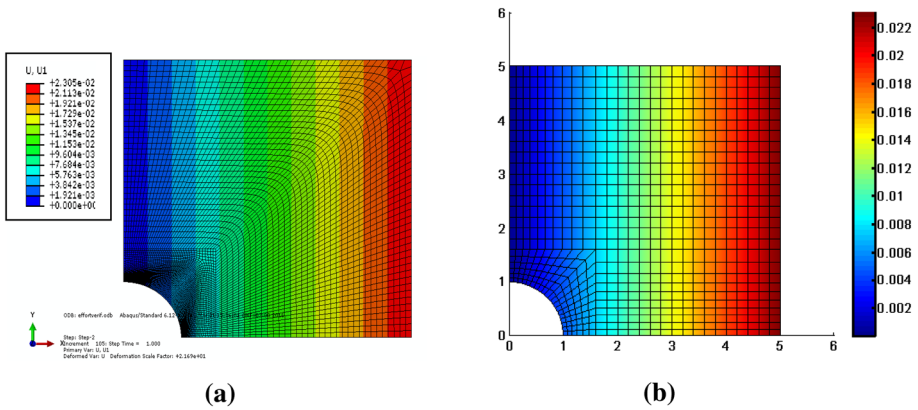


Fig. 14 u_x evolution all over the plate for FEM method (a) and IEFG method (b)

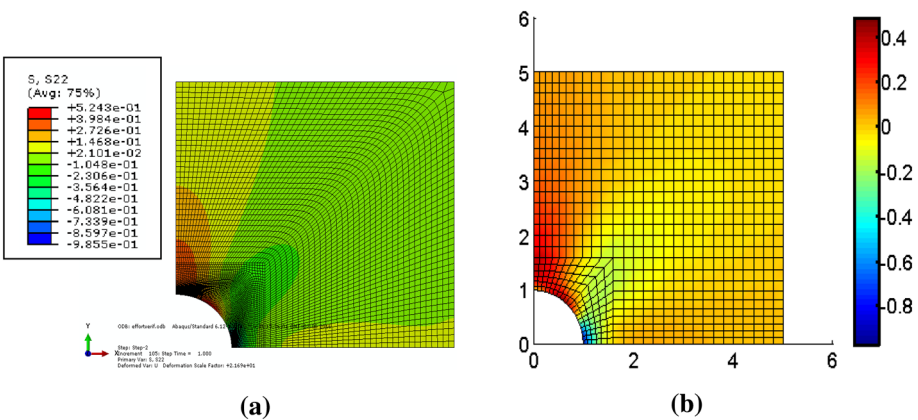


Fig. 15 σ_{22} evolution all over the plate for FEM method (a) and IEFG method (b)

5 Conclusions

In the present paper, the IIEFG method is presented for the analysis of linear thermo-elasticity. This mesh-free method which is a combination between the IMLS approximation and the EFG method does not have the delta Kronecker property, so that penalty technique is used to impose essential boundary conditions. Linear thermo-elasticity is solved in two steps: first, heat transfer problem is solved to get temperature field, and then, this latter is used in thermo-elastic problem as input to reach displacement and stress fields. The capacity of the IIEFG to treat linear thermo-elasticity is proved using 2D problems with both, regular and irregular node distributions. Numerical results, such as computed temperature, displacement, and stress, are in good agreement with analytic solution and reference FEM solution. Comparison shows that relative error norm given by the IIEFG is always under 6.24410^{-2} for stress and it is under 5.26710^{-4} for temperature and displacement. Therefore, the ability of the IIEFG to solve thermo-elastic problems is proved.

References

- Belytschko T, Lu YY (1994) Element-free Galerkin methods. *Int J Num Meth Eng* 37:229–256
- Bobaru F et al, Mukherjee S (2002) Meshless approach to shape optimization of linear thermoelastic solids. *Int J Num Meth Eng* 53:765–796
- Bouhala L, Makradiand A (2012) Thermal and thermo-mechanical influence on crack propagation using an extended mesh free method. *Eng Frac Mech* 88:35–48
- Cheng RJ et al, Liew KM (2012) Analyzing modified equal width (MEW) wave equation using the improved element-free Galerkin method. *Eng Anal Bound Elem* 36:1322–1330
- Ching HK, Yen SC (2005) Meshless Local Petrov-Galerkin analysis for 2D functionally graded elastic solids under mechanical and thermal loads. *Composites: Part B* 36:223–240
- Ching H, Chen J (2007) Thermomechanical analysis of functionally graded composites under laser heating by the MLPG method. *Comput Model Eng Sci* 2(4):633–653
- Debbabi I, Sendi Z et al (2015) Element Free and Improved Element Free Galerkin Methods for One and Two-Dimensional Potential Problems. *Design Model Mech Syst-I*
- Feng SZ, Cui XY (2013) Analysis of transient thermo-elastic problems using edge-based smoothed finite element method. *Int J Therm Sci* 65:127–135
- Hibbitt HD, Marcal PV (1973) A numerical, thermo-mechanical model for the welding and subsequent loading of a fabricated structure. *Comp Struct* 3(5): 1145–1174
- Huebner KH, Dewhirst DL et al (2008) *The finite element method for engineers*. AlBazaar
- Liew KM,) Cheng YM et al (2005) Boundary element-free method (BEFM) for two-dimensional elastodynamic analysis using Laplace transform. *Int J Num Methods Eng* 64(12):1610–1627
- Li H, Shantanu S. Mulay (2013) *Meshless methods and their numerical properties*. CRC Press, Taylor and Francis Group
- Liu Gr (2003) *Mesh free methods: moving beyond the finite element method*. CRC Press LLC
- Pant M, Singh IV et al (2010) Numerical simulation of thermo-elastic fracture problems using element free Galerkin method *Int J Mech Sci* 52(12):1745–1755
- Pant M, Singh IV et al (2011) A numerical study of crack interactions under thermo-mechanical load using EFGM. *J Mech Sci Tech* 25(2):403–413
- Parkus H (1968) *Thermoelasticity*, second edn., Springer 3-211-81375-6
- Pathak H, Singh A et al (2013) Fatigue Crack Growth Simulations of Bi-material Interfacial Cracks under Thermo-Elastic Loading by Extended Finite Element Method. *Eur J Comp Mech* 22(1):79–104
- Pathak H, Singh A et al (2014) Fatigue crack growth simulations of homogeneous and bi-material interfacial cracks using element free Galerkin method. *Ap Math Mod* 38:3093–3123
- Reza Eslami M (2014) *Finite Elements Methods in Mechanics*. Springer
- Sladek J, Sladek V, Atluri SN (2001) A Pure Contour Formulation for the Meshless Local Boundary Integral Equation Method in Thermoelasticity. *Comp Mod Eng Sci* 2:423–433
- Takeuti Y, Furukawa T (1981) Some Considerations on Thermal Shock Problems in a Plate. *J Appl Mech* 48(1):113–118

- Zeng H, Peng L et al. (2011) Dispersion and pollution of the improved meshless weighted least-square (IMWLS) solution for the Helmholtz equation. *Eng Anal Bound Elem* 35:791–801
- Zenkour AM, Abbas IA (2014) A generalized thermoelasticity problem of an annular cylinder with temperature-dependent density and material properties. *Int J Mech Sci* 84:54–60
- Zhang LW, Liew KM (2014) An improved moving least-squares Ritz method for two-dimensional elasticity problems. *App Math Comp* 246:268–282
- Zhang Z, Wang JF, et al (2013) The improved element-free Galerkin method for three-dimensional transient heat conduction problems. *Sci China Phys Mech Astro* 56(8):1568–1580
- Zhang Z, Zhao P et al (2009) Improved element-free Galerkin method for two-dimensional potential problems. *Eng Anal Bou Elem* 33:547–554
- Zheng BJ, Gao XW et al (2015) A novel meshless local Petrov–Galerkin method for dynamic coupled thermoelasticity analysis under thermal and mechanical shock loading. *Eng Anal Bou Elem* 60:154–161
- Zhu T, Atluri SN (1998) A modified collocation method and a penalty formulation for enforcing the essential boundary conditions in the element free Galerkin method. *Comp Mech* 21:211–222